Prognostics Enhanced Reconfigurable Control of Electro-Mechanical Actuators

Douglas W. Brown [1], George Georgoulas [1], Brian Bole [1], Hai-Long Pei [2], Marcos Orchard [3], Liang Tang [4], Bhaskar Saha [5], Abhinav Saxena [5], Kai Goebel [5], and George Vachtsevanos [1]

[1] *Department of Electrical and Computer Engineering, Georgia Institute of Technology, Atlanta, GA, 30332, USA.*
dbrown31@gatech.edu
gjv@ece.gatech.edu
[2] *Department of Automation at South China University of Technology, Guangzhou 510640 P.R. China.*
auhlpei@scut.edu.cn
[3] *Department of Electrical Engineering, Universidad de Chile, Santiago, Chile.*
morchard@ing.uchile.cl
[4] *Impact Technologies, LLC., Rochester, NY 14623, USA.*
Liang.Tang@impact-tek.com
[5] *NASA Ames Research Center, Moffett Field, CA 94035, USA.*
kai.goebel@nasa.gov

ABSTRACT

Actuator systems are employed widely in aerospace, transportation and industrial processes to provide power to critical loads, such as aircraft control surfaces. They must operate reliably and accurately in order for the vehicle / process to complete successfully its designated mission. Incipient actuator failure conditions may severely endanger the operational integrity of the vehicle / process and compromise its mission. The ability to maintain a stable and credible operation, even in the presence of incipient failures, is of paramount importance to accomplish "must achieve" mission objectives. This paper introduces a novel methodology for the fault-tolerant design of critical subsystems, such as an Electro-Mechanical Actuator (EMA), that takes advantage of on-line, real-time estimates of the Remaining Useful Life (RUL) or Time-to-Failure (TTF) of a failing component and reconfigures the available control authority by trading off system performance with control activity. The primary goal is to complete critical mission objectives within a time window dictated by prognostic algorithms so that the fault mode is accommodated and an acceptable level of performance maintained for the duration of the mission. The proposed fault-tolerant control design is mathematically rigorous, generic and applicable to a variety of application domains. An EMA is used to illustrate the efficacy of the proposed approach.

1 INTRODUCTION

The emergence of complex and autonomous systems, such as modern aircraft, Unmanned Aerial Vehicles (UAVs), automated industrial processes, among many others, is driving the development and implementation of new control technologies that are aimed to accommodate incipient failures and maintain a stable system operation for the duration of the emergency. Historically, when fault tolerance was an issue, controllers were designed targeting specific faults and specific control actions to accommodate the corresponding faults (Isermann, 1984). More recent approaches applied modern control techniques such as adaptive or robust control to handle situations where the fault severity may not be known, but the system structure is known. While these techniques are capable of handling many types of fault modes, they do so in a brute force way (Saberi *et al.*, 2000). For example, if a fault condition can be modeled as a change in system parameters, an adaptive controller can be designed to monitor the changes and constantly change the control law accordingly (Ward *et al.*, 2001; Monaco *et al.*, 2004). Similarly, a robust control law may be designed which can control the system over a range of potential failure modes (Stoustrup *et al.*, 1997; Zhou *et al.*, 1996). However, what these approaches lack is an active reconfiguration of the control law considering failure prognostic information. Fault-Tolerant Control (FTC) methodologies typically have two main objectives: Fault Detection and Isolation (FDI) and Control Reconfiguration (Rausch *et al.*, 2007). Several authors have reported on the problem of FDI (Kleer and Williams, 1987; Filippetti *et al.*, 2000; Skormin *et al.*, 1994; Willsky, 1976; Wu *et al.*, 2004). Analytical methods for FTC usually assume linear models of the system dynamics. For large-scale systems, this is generally a reasonable assumption since in a region of the nominal operating point, the system dynamics are approximately linear. Recent research has begun to address the issue of FTC for nonlinear systems, such as using feedback linearization in a restructured digital flight control system (Nguyen and Liu, 1998). The authors in (Birdwell *et al.*, 1986; Birdwell, 1978) describe a method for reliable control system design. Reliability is defined as the probability that a system will perform within specified constraints for a given period of time. In (Watanabe and Himmelblau, 1982), the author discusses several issues arising in the design of reconfigurable control systems including the selection of a failure representation method, the selection of a control law that provides robustness to particular failures and the formulation of a diagnostic problem that exploits potentialities in a control system for diagnostic purposes. Additional contributions significant to the development of adaptive based FTC can be found in (Ye and Yang, 2006; Zhang and Jiang, 2003). The authors in (Yavrucuk *et al.*, 1999) present a novel simultaneous FDI and FTC strategy. Other recent analytical approaches employ a mathematical model in which failures are captured as uncertainties in the model parameters (Mufti and Vachtsevanos, 1995), or controller reconfiguration is affected by considering the redirection of control authority between parts of the system (Bajpai *et al.*, 2001). Artificial Intelligence (AI) methods have been exploited to handle model-free fault diagnosis and FTC in an expert system setting (Levis, 1987; Isermann, 1997). Recent extensions to expert system approaches to fault tolerance include (Wu, 1997), in which past performance is used to dynamically update the database of fault controllers / parameters. An alternative hybrid systems approach to FTC combines modeling with AI and expert systems (Heck *et al.*, 2003). Many existing reconfigurable control strategies fall naturally into this category (Boskovic and Mehra, 2001; Liu, 1996). More recently, hybrid hierarchical approaches to FTC have been proposed (Vachtsevanos *et al.*, 2005; Gutierrez *et al.*, 2003; Guler *et al.*, 2003; Kamen *et al.*, 1994). For example, in (Clements, 2003), the high-level of the architecture includes situation awareness and fault diagnosis routines, whereas the middle-level consists of three modules that actively reconfigure the controls, subsystem interconnections and local controller gains; the low-level consists of the individual subsystems and corresponding local controller (Clements *et al.*, 2000). In another manifestation, the high level performs mission adaptation functions (Drozeski and Vachtsevanos, 2005; Drozeski *et al.*, 2005; Tang *et al.*, 2008).

In contrast to FTC, little work has been published discussing the role of prognosis in control systems. In, (Bogdanov *et al.*, 2006; Gokdere *et al.*, 2006) the authors describe a framework to consider long-term lifetime prediction, performance and design constraints. To account for the lifetime constraint, the authors consider a parametrization of a family of LQR controllers with a single adaptation parameter, and then optimize the parameter to satisfy the lifetime constraint. Although novel, more work is required in the area of prognostic-based control to handle uncertainties associated with long-term prediction.

This paper is organized as follows. Section 2.1 identifies the EMA under investigation and presents a general overview of the FTC architecture; Section 3 introduces a particle filtering framework for *fault diagnosis* and *fault prognosis* and follows using an EMA with a selected failure mode as an example; Section 4 gives a formulation for a prognosis-based control law utilizing Model Predictive Control (MPC) and evaluates the feasibility of the approach using the EMA example; Section 5 highlights major accomplishments.

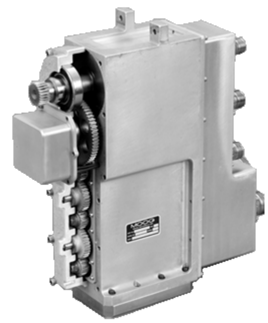

Figure 1: Photo of the triplex redundant EMA.

2 BACKGROUND

2.1 Actuator subsystem

The actuator evaluated for proof of concept of the proposed fault-tolerant or reconfigurable control scheme is a triplex redundant rotary EMA, designed to operate with a triplex redundant Electronic Control Module (ECM). The EMA, shown in Figure 1, consists of three Brushless DC (BLDC) motors, each using a resolver for motor commutation, where all motors are driving a single string output shaft drive mechanism through a gear system (Brown *et al.*, 2009).[1] This actuator is suitable for this study since it can operate in a single channel (simplex) mode or in fully redundant, active-active-active system mode, providing a two fault-tolerant system. In the active-active-active system, all three motors are actively driven in a torque sharing mode where the torque applied to the load is the cumulative sum of the three motor torques. A Vehicle Management Computer (VMC) determines the drive for each motor/channel and the corresponding servo controllers. The VMC also monitors each motor channel for failures or degraded performance, so it can shut it down when necessary. A block diagram of the nominal system illustrating the production controller and three motor components is depicted in Figure 2.

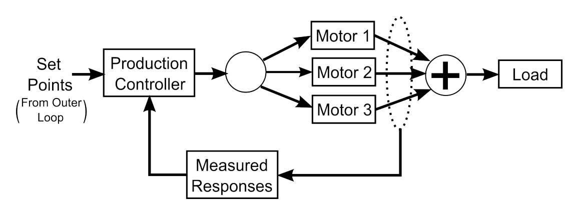

Figure 2: Block diagram of the triplex redundant EMA.

[1]Copyright © Moog Inc. Photo courtesy of Moog Inc.

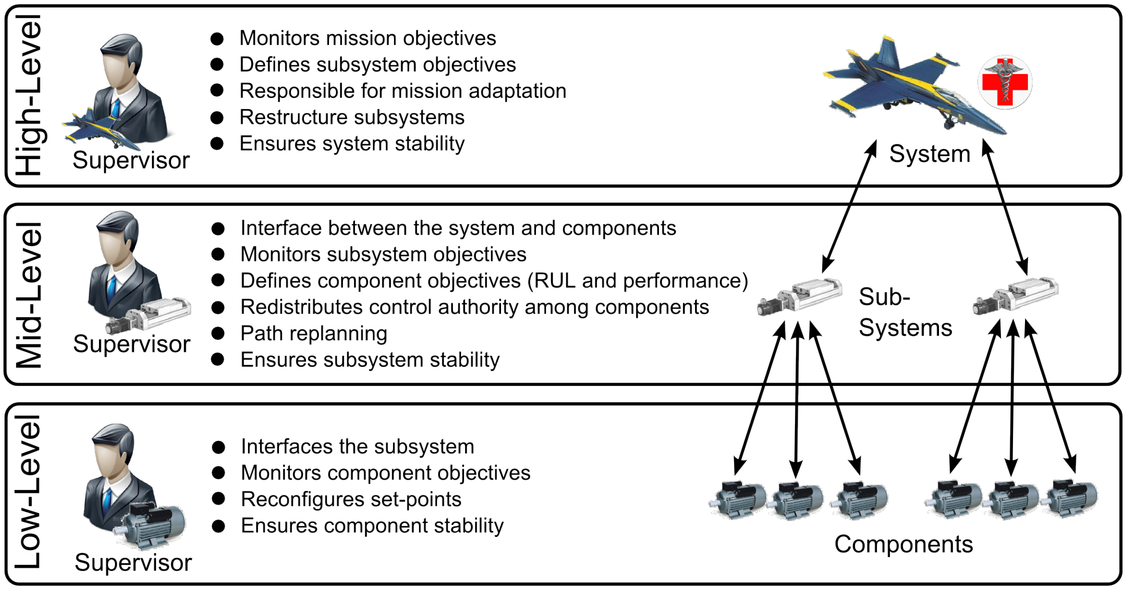

Figure 3: Reconfigurable control architecture 3-tier hierarchical strategy.

2.2 Fault-Tolerant Control Architecture

The reconfigurable control methodology introduced in this paper is a constituent module of a more general intelligent / hierarchical FTC architecture comprised of three levels: A *low-level*, a *middle-level* and a *high-level*, as illustrated in Figure 3. Each level of the control hierarchy is responsible for different tasks where the three levels are coordinated via supervisory routines and contribute synergistically to system fault tolerance.

Figure 4 depicts the main elements of the low-level reconfigurable control architecture. The control architecture is comprised of two controllers: the original *production controller* (§1030) and the *reconfigured controller* (§1040). Initially, the production controller is utilized while diagnostic routines continuously monitor the system for one, or more, fault modes (§1100). Once a fault is detected the RUL requirements are check to assess if the mission can be accomplished without control reconfiguration (§1300), if not, the MPC routine is called upon (§1400).

The functionality of the MPC routine is given by the flowchart in Figure 5. Soft constraints are initialized (§1410), the RUL of the failing motor is evaluated (§1420) and the RUL requirements are checked (§1430) to assess if the mission can be accomplished; if not, the soft constraints are updated to relax performance requirements in the MPC (§1450). Then, the MPC computes the next control sequence (§1460). After the control sequence is applied, the performance is evaluated (§1470) and compared to the required performance (§1440). If the performance requirements are satisfied the control sequence is reiterated (§1490). However, if the requirements are not satisfied, or the soft boundaries can no longer be adapted (§1440), a control redistribution algorithm (§1500) is activated at the middle-level of the control hierarchy.

It should be noted that control redistribution is not

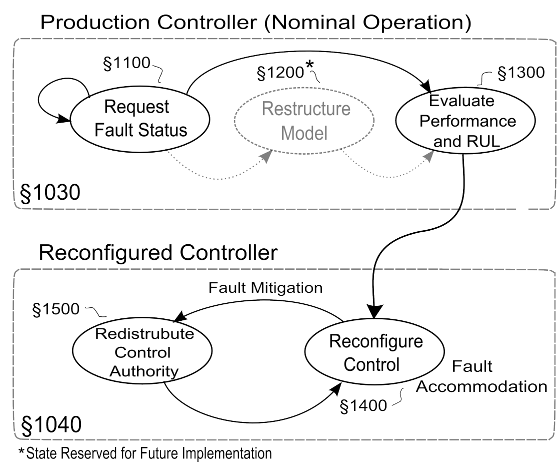

Figure 4: State transition diagram for low-level reconfigurable control.

addressed in this paper. Also, it is assumed that, in the presence of an incipient failure, the system (actuator) dynamics remain essentially the same. This assumption is valid when the incipient failure or fault is detected at an early stage of its initiation and evolution and thus has not affected severely the actuator dynamics. Under these conditions, restructuring of the system dynamics is not absolutely necessary in the control formulation. However, if the motor fault significantly influences the system dynamics, then a restructuring step (§1200) can precede the reconfigurable control routine so the current state of the system is reflected in the control formulation.

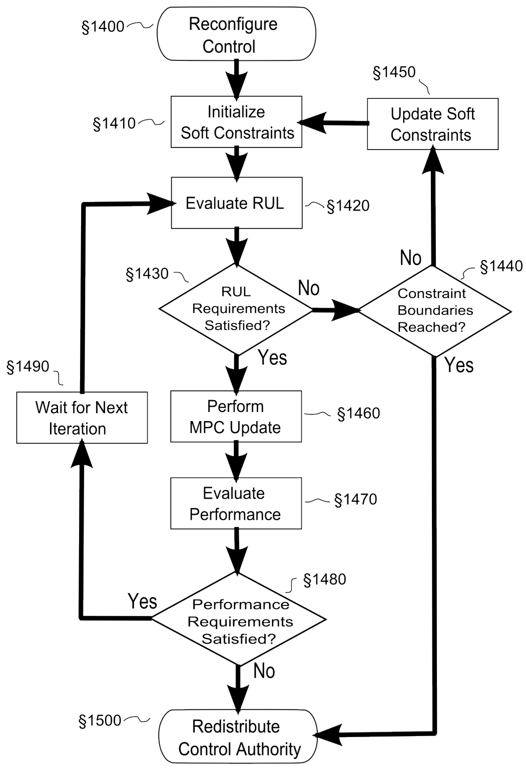

Figure 5: Flowchart of the reconfiguration state.

3 FAULT DETECTION AND FAILURE PROGNOSIS

3.1 Actuator Model

A high-fidelity 5th order state-space model was developed to represent higher order dynamics for a closed-loop actuator position controller. The model, which can be expressed by the linear state-space system $(\mathbf{A}_m, \mathbf{B}_m, \mathbf{C}_m)$, is employed to relate the control inputs and measured outputs of the actuator to the internal system states of the BLDC motor,

$$\left\{ \begin{array}{lcl} \dot{\tilde{\mathbf{x}}}_m & = & \mathbf{A}_m \tilde{\mathbf{x}}_m + \mathbf{B}_m \mathbf{u}_m \\ \mathbf{y}_m & = & \mathbf{C}_m \tilde{\mathbf{x}}_m \end{array} \right. \tag{1}$$

where $\tilde{\mathbf{x}}_{m0} = \tilde{\mathbf{x}}_\mathbf{m}(0)$. The internal state $\tilde{\mathbf{x}}_m = [\, \tilde{i}_m \quad \tilde{\theta}_m \quad \tilde{\omega}_m \quad \tilde{\theta}_\ell \quad \tilde{\omega}_\ell \,]^\top \in \mathbb{R}^5$ is defined by the motor current, motor position, motor speed, load position and load speed, respectively; the control input $\mathbf{u}_m = [\, \theta_{ref} \quad T_{load} \,]^\top \in \mathbb{R}^2$ is defined by the reference position and external load disturbance; and the control output $\mathbf{y}_m = [\, \theta_\ell \quad i_m \,]^\top \in \mathbb{R}^2$ is defined by the load position and motor current.

The transition matrix, $\mathbf{A}_m \in \mathbb{R}^{5\times 5}$, is defined as a piecewise linear model,

$$\mathbf{A}_m = \left\{ \begin{array}{lcl} \mathbf{A}_1 & : & \tilde{\omega}_m \geq 0 \\ \mathbf{A}_2 & : & \tilde{\omega}_m < 0 \end{array} \right. \tag{2}$$

where the matrices $\mathbf{A}_1$ and $\mathbf{A}_2 \in \mathbb{R}^{5\times 5}$ are defined in (3) and (4) accordingly.

$$\mathbf{A}_1 = \begin{bmatrix} \frac{-R_{tt}}{L_{tt}} & \frac{-k_{p1}k_{p2}}{L_{tt}} & \frac{-k_e - k_{p1}}{L_{tt}} & 0 & 0 \\ 0 & 0 & 1 & 0 & 0 \\ \frac{k_t}{J_m} & \frac{-k_{cs}}{J_m N_{cm}^2} & \frac{-b_m - T_f}{J_m} & \frac{k_{cs} N_{cl}}{J_m N_{cm}} & 0 \\ 0 & 0 & 0 & 0 & 1 \\ 0 & \frac{k_{cs} N_{cl}}{J_\ell N_{cm}} & 0 & \frac{-k_\ell - k_{cs} N_{cl}^2}{J_\ell} & \frac{-b_\ell}{J_\ell} \end{bmatrix} \tag{3}$$

$$\mathbf{A}_2 = \begin{bmatrix} \frac{-R_{tt}}{L_{tt}} & \frac{-k_{p1}k_{p2}}{L_{tt}} & \frac{-k_e - k_{p1}}{L_{tt}} & 0 & 0 \\ 0 & 0 & 1 & 0 & 0 \\ \frac{k_t}{J_m} & \frac{-k_{cs}}{J_m N_{cm}^2} & \frac{-b_m + T_f}{J_m} & \frac{k_{cs} N_{cl}}{J_m N_{cm}} & 0 \\ 0 & 0 & 0 & 0 & 1 \\ 0 & \frac{k_{cs} N_{cl}}{J_\ell N_{cm}} & 0 & \frac{-k_\ell - k_{cs} N_{cl}^2}{J_\ell} & \frac{-b_\ell}{J_\ell} \end{bmatrix} \tag{4}$$

The control and observation matrices $\mathbf{B}_m \in \mathbb{R}^{5\times 2}$ and $\mathbf{C}_m \in \mathbb{R}^{2\times 5}$ are defined in (5) and (6), respectively.

$$\mathbf{B}_m = \begin{bmatrix} \frac{k_{p1}k_{p2}N_{cm}}{L_{tt}N_{cl}} & 0 & 0 & 0 & 0 \\ 0 & 0 & 0 & 0 & \frac{-1}{J_\ell} \end{bmatrix}^\top \tag{5}$$

$$\mathbf{C}_m = \begin{bmatrix} 0 & 0 & 0 & 1 & 0 \\ 1 & 0 & 0 & 0 & 0 \end{bmatrix} \tag{6}$$

3.2 Failure Modes and Effects

Results from a Failure Modes and Effects Criticality Analysis (FMECA) study of the EMA suggest that the leading modes of failure are associated with the bearings (Schoen *et al.*, 1995; Zhang *et al.*, 2008a; Bodden *et al.*, 2007), position feedback sensors (Murray *et al.*, 2002; Brown *et al.*, 2008), electronic components (Baybutt *et al.*, 2008) and electric motors (Brown *et al.*, 2008; 2009). In this study, the BLDC motor was selected as the component of interest where the primary failure mechanisms is breakdown of insulation between turns of the same winding. According to (Malik *et al.*, 1998; Nandi and Toliyat, 1999; Tavner and Penman, 1987), stator insulation can fail due to several reasons: high stator core or winding temperature; contamination from oil, moisture and dirt; short circuit or starting stresses; electrical discharges; and leaking in the cooling system. For the EMA under investigation, winding temperature is the dominant failure mechanism due to the excessive environmental factors.

The principle effects of a turn-to-turn winding insulation short result in a three-phase impedance imbalance in the stator windings (Xianrong *et al.*, 2003). This leads to asymmetries in the stator phase currents, shown in Figure 6, resulting in increased harmonic generation and overall performance degradation (Penman *et al.*, 1994).

3.3 Particle Filtering in Real-Time Fault Diagnosis and Failure Prognosis

Particle filtering is an emerging and powerful methodology for sequential signal processing with a wide rage of applications in science and engineering. Founded on the concept of sequential importance sampling and the use of Bayesian theory, particle filtering is particularly useful in dealing with difficult nonlinear and/or

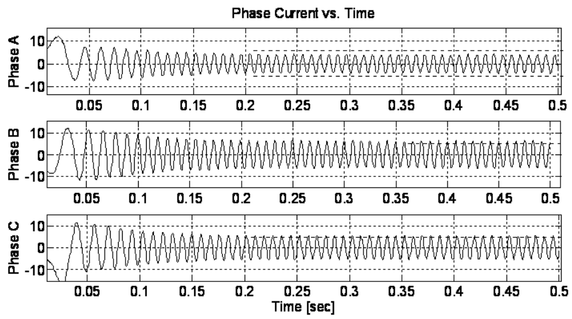

Figure 6: Simulation illustrating phase current asymmetry.

non-Gaussian problems. The underlying principle of the methodology is the approximation of relevant distributions with particles (samples from the space of the unknowns) and their associated weights. Compared to classical Monte-Carlo methods, sequential importance sampling enables particle filtering to reduce the number of samples required to approximate the distributions with necessary precision, and makes it a faster and more computationally efficient approach than Monte-Carlo simulation. This is of particular benefit in diagnosis and prognosis of complex dynamic systems, such as engines, gas turbines and gearboxes, because of the nonlinear behavior when operating under fault conditions. Moreover, particle filtering allows information from multiple measurement sources to be fused in a principled manner (Orchard, 2007).

Particle filtering has a direct application in the FDI arena. Once the current state of the system is known, it is natural to implement FDI procedures by comparing the process behavior with patterns regarding normal or faulty operating conditions.

3.4 Fault Diagnosis

A fault diagnosis procedure involves the tasks of fault detection, fault isolation and identification (assessment of the severity of the fault). The proposed particle-filter-based diagnosis framework aims to accomplish these tasks, under general assumptions of non-Gaussian noise structures and nonlinearities in process dynamic models, using a reduced particle population to represent the state pdf (Orchard *et al.*, 2008). A compromise between model-based and data-driven techniques is accomplished by the use of a particle filter-based module built upon the nonlinear dynamic state model,

$$\left\{ \begin{array}{rcl} x_d\left(t+1\right) & = & f_b\left(x_d\left(t\right), n\left(t\right)\right) \\ x_c\left(t+1\right) & = & f_t\left(x_d\left(t\right), x_c\left(t\right), w\left(t\right)\right) \\ f_p\left(t\right) & = & h_t\left(x_d\left(t\right), x_c\left(t\right), v\left(t\right)\right) \end{array} \right. \tag{7}$$

where f_b, f_t and h_t are non-linear mappings, x_d is a collection of Boolean states associated with the presence of a particular operating condition in the system (normal operation, fault type #1, #2, etc.), x_c is a set of continuous-valued states that describe the evolution of the system given those operating conditions, f_p is a feature measurement, ω and v are non-Gaussian distributions that characterize the process and feature noise signals, respectively. The function h_t is a mapping between the feature value, $f_p\left(t\right)$, and the fault state $x_c\left(t\right)$. In the case of a turn-to-turn winding insulation short circuit fault, the values of $f_p\left(t\right)$ and $L\left(t\right)$ are related by the operating parameters, motor speed, ω_m and motor current, i_m, as will be shown explicitly in a future publication. For simplicity, $n\left(t\right)$ may be assumed to be zero-mean i.i.d. uniform white noise. At any given instant of time, this framework provides an estimate of the probability masses associated with each fault mode, as well as a pdf estimate for meaningful physical variables in the system. Once this information is available within the FDI module, it is processed to generate proper fault alarms and to inform about the statistical confidence of the detection routine. Furthermore, pdf estimates for the system continuous-valued states (computed at the moment of fault detection) may be used as initial conditions in failure prognostic routines. As a result, a swift transition between the two modules (FDI and prognosis) may be performed and reliable prognosis can be achieved within a few cycles of operation after the fault is declared. This characteristic is one of the main advantages of the proposed particle-filter-based diagnosis framework. Customer specifications are translated into acceptable margins for the type I and/or II errors, as defined by (Kutner *et al.*, 2004; Hines *et al.*, 2003), in the detection routine. The algorithm itself will indicate when the type II error (false negatives) has decreased to the desired level. Figure 7 depicts the major modules of the proposed architecture for a fault detector.

In this architecture, real-time measurements and information about the current operational mode are provided on-line. Then data is pre-processed and denoised before computing the features that will assist to efficiently monitor the behavior of the system. By taking the standard deviation of the average amplitude of each phase current (a, b and c) over a finite time interval T, the following feature, denoted as $f_p\left(t\right)$, can be used to describe variations in winding symmetry for a BLDC motor (Brown *et al.*, 2009),

$$f_p\left(t\right) = \underset{k\in(a,b,c)}{\operatorname{std}} \left[\underset{t\in(0,T)}{\operatorname{avg}} \left| i_k\left(t\right) + \hat{i}_k\left(t\right) \right| \right] \tag{8}$$

where the symbol i_k, refers to the measured phase current and $\hat{i}_k$ corresponds to the phase current after applying a Hilbert transformation. Provided in Figure 8 is a (a) snapshot of experimental data acquired during seeded fault testing and (b) a plot of computed features versus time. The feature value $f_p\left(t\right)$ is computed from raw current data. The fault dimension $L\left(t\right)$ was simulated by placing a parallel resistance between one of the winding terminals and the center-tap, thereby generating current asymmetry. The parallel resistances used ranged from 25Ω to 3Ω and decreasing monotonically with time. As the parallel resistance decreased, the fault dimension $L\left(t\right)$ increased, resulting in an increase in $f_p\left(t\right)$. More detailed information regarding the seeded fault winding insulation test can be found in (Brown *et al.*, 2009).

It should be noted that the principle feature, $f_p\left(t\right)$, is not the only available feature. Other diagnostic features for turn-to-turn winding insulation faults were

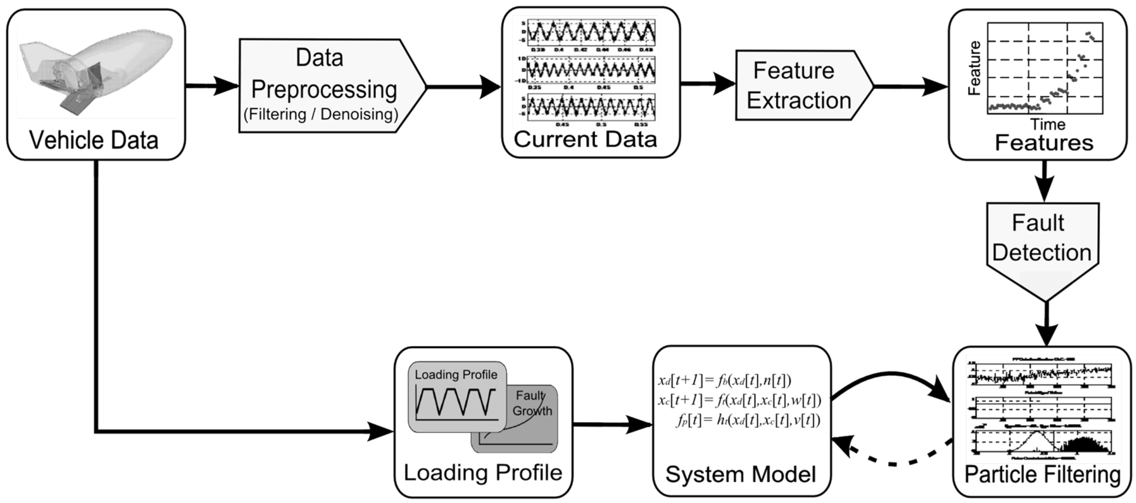

Figure 7: Particle filter-based fault detection architecture.

also considered and may be used individually or in combination via fusion techniques.

Statistical analysis applied to this set of features is performed to simultaneously arrive at the probability of abnormal conditions for a given false alarm rate and confidence level (95% for example). If time and computational resources allow for further analysis, feature information can be used to complete the tasks of fault isolation, identification, and failure prognosis (Zhang *et al.*, 2008b). The fault detector was evaluated using simulated phase currents generated in Simulink. The results of the particle-filter based fault detector using experimental data from Figure 8 (a) are provided in Figure 9 showing (a) the raw output from the particle filter over time as a waterfall plot and (b) the corresponding fault detection confidence. The critical feature value, $f_{p,\alpha=0.05} = 0.02$ was computed for a 5% false alarm rate ($\alpha = 0.05$ / type I error) using the initial baseline data. The confidence was computed by summing all the weights associated with particles greater than $f_{p,\alpha=0.05}$. In this paper, confidence is defined as the compliment of the Type II error, β, expressed as a percentage,

$$\text{Confidence} = 100\% \, (1 - \beta) \tag{9}$$

3.5 Failure Prognosis

Prognosis is the Achilles' heel of fault diagnosis and failure prognosis systems. Prognosis can be understood as the generation of long-term predictions describing the evolution in time of a particular signal of interest or fault indicator. Since prognosis projects the current condition of the indicator in the absence of future measurements, it necessarily entails large-grain uncertainty. This suggests a prognosis scheme based on recursive Bayesian estimation techniques, combining both the information from fault growth models and on-line data obtained from sensors monitoring key fault parameters (observations or features). Proposed is a prognostic framework that takes advantage of a nonlinear process (fault / degradation) model, a Bayesian estimation method using particle filtering and real-time measurements.

Prognosis is achieved by performing two sequential steps, *prediction* and *filtering*. Prediction uses both the knowledge of the previous state estimate and the process model to generate the a priori state pdf estimate for the next time instant,

$$p\left(x_{0:t}|y_{1:t-1}\right) = \int p\left(x_t|x_{t-1}\right) p\left(x_{0:t-1}|y_{1:t-1}\right) dx_{0:t-1} \tag{10}$$

The filtering step generates the posterior state pdf by using Bayes formula,

$$p\left(x_{0:t}|y_{1:t-1}\right) \propto p\left(y_t|x_t\right) p\left(x_t|x_{0:t-1}\right) p\left(x_{0:t-1}|y_{1:t-1}\right) \tag{11}$$

Expressions (10) and (11) do not have an analytical solution in most cases. Instead, Sequential Monte Carlo (SMC) algorithms, or particle filters, are used to numerically solve (10) and (11) in real-time through the use of efficient sampling strategies (Arulampalam *et al.*, 2002; Doucet *et al.*, 2000). Particle filtering approximates the state pdf using samples of "particles" having associated discrete probability masses ("weights") as,

$$p\left(x_t|y_{1:t}\right) \approx \sum_{i=1}^{N} \tilde{w}_t\left(x_{0:t}^i\right) \cdot \delta\left(x_{0:t} - x_{0:t}^i\right) \tag{12}$$

where $x_{0:t}^i$ is the state trajectory and $y_{1:t}$ are the measurements up to time t. The simplest implementation of this algorithm, the Sequential Importance Resampling (SIR) particle filter, updates the weights using the likelihood of y_t as (Orchard, 2007; Orchard *et al.*, 2008),

$$w_t = w_{t-1} \cdot p\left(y_t|x_t\right) \tag{13}$$

By using the state equation to represent the evolution of the fault dimension in time, it is possible to generate a long-term prediction for the state pdf, in the absence of new measurements, in a recursive manner using the

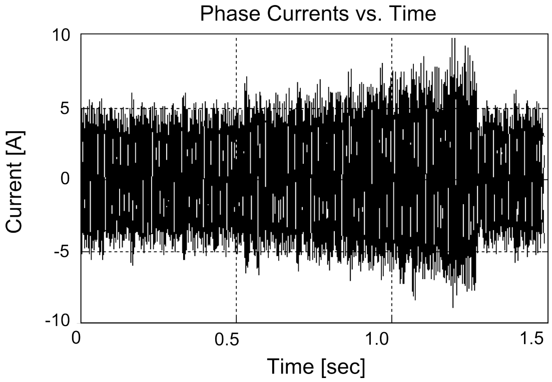

(a)

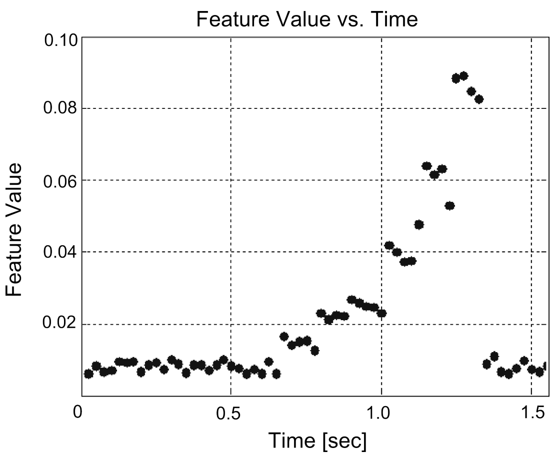

(b)

Figure 8: Plot of (a) three-phase current data and (b) features computed from experimental data.

current pdf estimate for the state,

$$\tilde{p}\left(x_{t+p}|y_{1:t}\right) \approx \int \tilde{p}\left(x_t|y_{1:t}\right) \prod_{j=t+1}^{t+p} p\left(x_j|x_{j-1}\right) dx_{t:t+p-1} \tag{14}$$

which can be approximated as,

$$\tilde{p}\left(x_{t+p}|y_{1:t}\right) \approx \sum_{i=1}^{N} w_t^{(i)} \int \cdots \int \tilde{p}\left(x_{t+1}|x_t^{(i)}\right) \cdot \ldots \prod_{j=t+2}^{t+p} p\left(x_j|x_{j-1}\right) dx_{t+1:t+p-1} \tag{15}$$

The information about the distribution of the state for future time instants is given by the position of the particles, not by the particle weight value. A computationally affordable solution is based on the use of kernel transitions and Monte Carlo resampling techniques for the state pdf,

$$\hat{p}\left(x_{t+k}|\hat{x}_{1:t+k-1}\right) \approx \sum_{i=1}^{N} w_{t+k-1}^{(i)} K\left(x_{t+k} - E\left[x_{t+k}^{(i)}|\hat{x}_{t+k-1}\right]\right) \tag{16}$$

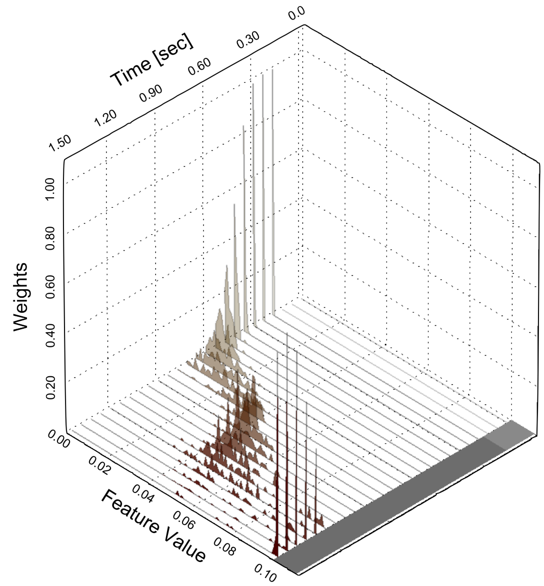

(a)

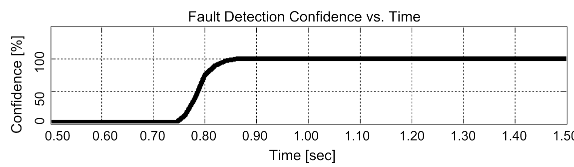

(b)

Figure 9: Fault detection using experimental data. Illustrated are (a) the results after applying a particle filter to the incoming feature and (b) the level of confidence computed from the particle weights.

Long-term predictions are used to estimate the probability of failure in a system given a hazard zone that is defined via a probability density function with lower and upper bounds for the domain of the random variable, denoted as H_{lb} and H_{up}, respectively.

The probability of failure at any future time instant is estimated by combining both the weights $w_{t+k}^{(i)}$ of predicted trajectories and specifications for the hazard zone through the application of the Law of Total Probabilities. The resulting RUL pdf, $\hat{p}_{t_{\mathrm{RUL}}}$, provides the basis for the generation of confidence intervals and expectations for prognosis,

$$\hat{p}_{t_{\mathrm{RUL}}} = \sum_{i=1}^{N} p\left(\mathrm{Fail}|X = \hat{x}_{t_{\mathrm{RUL}}}^{(i)}, H_{lb}, H_{up}\right) \cdot w_{\mathrm{RUL}}^{(i)} \tag{17}$$

Fault Growth Model

The motor winding insulation degrades at a rate related to the winding temperature, T_w. The fault-growth rate can be related to temperature through Arrhenius' law (Gokdere *et al.*, 2006),

$$\dot{L}\left(t\right) \propto \exp\left(-\frac{E_a}{k_B T_w}\right) \tag{18}$$

where the symbols E_a and k_B refer to the activation energy and Boltzmann's constant, respectively. However, this expression does not consider the current state of the fault dimension. By incorporating concepts from Paris' law (Paris and Gomez, 1961) into (18), the rate of degradation for the winding insulation fault is modeled as,

$$\dot{L} = \beta_0 exp\left(-\frac{E_a}{k_B T_w}\right) L \quad (19)$$

where $\beta_0 > 0$. This suggests that the rate of degradation is proportional to the fault dimension itself where the constant of proportionality follows a relationship with winding temperature according to Arrhenius law.

Thermal Model

In the case of the brushless DC motor, the winding temperature is related to the power loss in the copper windings. Note: this assumes the copper losses are the primary source of power loss. A model describing the relationship between the power loss and winding-to-ambient temperature, T_{wa}, as defined in (20), is shown in Figure 10 (Gokdere *et al.*, 2006; Nestler and Sattler, 1993). The symbols T_a, C_{wa} and R_{wa} refer to the ambient temperature, thermal capacitance and thermal resistance of the windings, accordingly.

$$T_{wa} = T_w - T_a \quad (20)$$

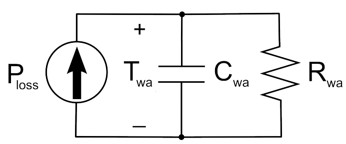

Figure 10: Schematic of the simplified thermal model.

The power loss is computed using (21), where i_k and R_k refer to the motor current and resistance of each winding phase ($k = 1, 2, 3$), respectively.

$$P_{\text{loss}} = \sum_{k=1}^{3} R_k i_k^2 \quad (21)$$

An equivalent state equation representation for Figure 7 can be written as,

$$\dot{T}_{wa} = \frac{P_{\text{loss}} R_{wa} - T_{wa}}{R_{wa} C_{wa}} \quad (22)$$

The unknown parameters in (22) can be identified using a linear reference model,

$$\dot{T}_{wa} = \hat{a}_m(t)\, T_{wa}(t) + \hat{b}_m(t)\, u(t) \quad (23)$$

where $u(t) = \sqrt{\frac{1}{3}\sum_{k=1}^{3} i_k^2}$. The unknown model parameters can be identified on-line in real-time by invoking an indirect Model Reference Adaptive Control (MRAC) scheme (Hovakimyan, 2008) using measurements for T_a, T_w, and u,

$$\begin{cases} \dot{\hat{a}}_m &= \gamma_a T_{wa} e(t) & \\ \dot{\hat{b}}_m &= \gamma_b u(t) e(t) & b_m > \bar{b} \\ & \gamma_b u(t) e(t) + \dfrac{\bar{b}_m - \hat{b}_m}{\hat{b}_m - \bar{b}_m + \epsilon} & b_m < \bar{b} \\ e(t) &= T_w(t) - T_a(t) - T_{wa} & \end{cases} \quad (24)$$

where $\gamma_a > 0$ and $\gamma_b > 0$ are adaptation gains, $\epsilon > 0$ is a sufficiently small number so that $\bar{b}_m - \epsilon > 0$ and the initialization of $\hat{b}(0) > \bar{b}_m$ is done with correct sign. It should be mentioned that (23) does not consider the non-linear effects that occur due to the thermal dependence of the winding resistance (Nave, 2008). Since the adaptation parameters, $\hat{a}_m$ and $\hat{b}_m$, vary slowly with time (22) provides a good localized estimate for C_{wa} and R_{wa}. However, a non-linear model would improve the accuracy of long-term predictions over a broader range of operating conditions.

Feature-Based Fault Growth Model

Prognosis requires the definition of a process model to incorporate information present in the feature data. Proposed in (25) is a fault / degradation growth state model, based on (19), for insulation degradation in a brushless DC motor. The state variable β is an unknown time-varying model parameter to be estimated. Additionally, the stochastic variables ω_1, ω_2 and v are represented using Gaussian distributions. Finally, the function h_t is a mapping between the feature value and fault dimension L.

$$\begin{cases} \dot{L}(t) &= \beta(t) \exp\left(-\frac{E_a}{k_B T_w}\right) L + \omega_1(t) \\ \dot{\beta}(t) &= \omega_2(t) \\ f_p(t) &= h_t(L(t), \omega_m, i_m) + v(t) \end{cases} \quad (25)$$

Long-term prediction of the failure evolution is based on an estimation of the current state and a model describing the fault progression, more specifically the fault-growth model. Once an incipient failure is detected and isolated, sensor data is collected to initialize the fault-growth model parameters used in the prognostic routines. Then, corrective terms are estimated in a learning paradigm to improve model parameter estimates and/or update the operating profiles thus resulting in better accuracy and precision of the algorithm for long-term prediction. Uncertainty associated with long-term predictions is managed, or reduced, by using the current state pdf estimate, process noise model, and a record of corrections made to previously computed predictions. In the first prognosis level, a $p-\mathrm{step}$ ahead prediction is generated on the basis of an a priori estimate, adjusting probabilities that are associated with the prediction according to the noise model structure. At the second prognosis level, these predictions are used to estimate the RUL pdf.

Particle filter-based prognosis was demonstrated for the turn-to-turn winding insulation fault using artificial data generated from the simulation model discussed earlier. A result showing the particle filter updates, diagnostic assessment and long-term predictions of RUL are provided in Figure 11.

4 RECONFIGURABLE CONTROL STRATEGY

The primary goal in this study is to introduce a reconfigurable controller to trade-off RUL for performance. In the case of the EMA, the RUL can be increased by lowering the applied motor current, i_m. Although, the motor current cannot be adjusted directly, it can be controlled indirectly by making adjustments to the reference input, θ_{ref}, shown in Figure 12. The purpose

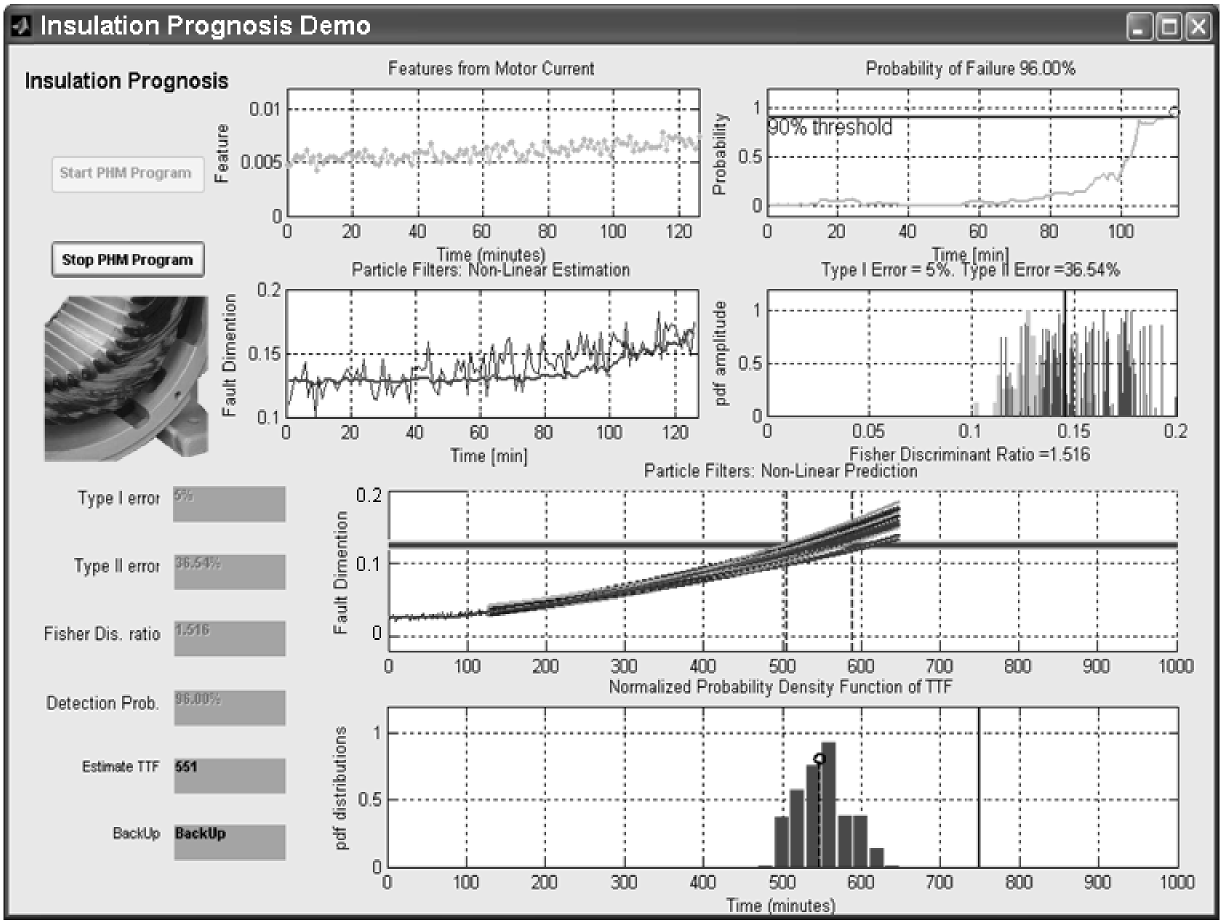

Figure 11: Example of particle filter based prognosis using artificial data.

of the MPC is to find the optimal $\tilde{\theta}_{\mathrm{ref}}$ for a given RUL and performance requirement.

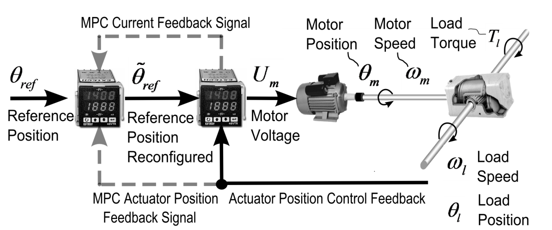

Figure 12: Block diagram showing actuator inputs and outputs

4.1 RUL Control Boundaries

The control input associated with a specific RUL value can be determined from the fault-growth model in (19). However, instead of using the particle filtering framework as mentioned earlier, the first approach utilizes an analytical expression for the expectation of the fault dimension. First, consider the equations that result from steady-state operating conditions for the motor current, winding-to-ambient temperature, and adaptation parameters $\bar{i}_m$, $\overline{T}_{wa}$, $\bar{a}_m$ and $\bar{b}_m$, respectively. Then, a steady-state equation can be written as,

$$\bar{a}_m \overline{T}_{wa} + \bar{b}_m \bar{i}_m^2 = 0 \tag{26}$$

where $u(t) = \sqrt{\frac{1}{3}\sum_{k=1}^{3} i_k^2}$. Next, the set of steady-state expressions from (25) can be used to write the expectation of the fault-growth dynamics in terms of the steady-state motor current and adaptation parameters,

$$\begin{cases} E\left[\dot{L}(t)\right] & = & \gamma_0 E\left[L(t)\right] \\ \gamma_0 & = & \overline{\beta}\exp\left(-\frac{E_a}{k_b \overline{T}_w}\right) \\ \overline{T}_w & = & T_a - \frac{\bar{b}_m \bar{i}_m^2}{\bar{a}_m} \end{cases} \tag{27}$$

Solving this differential equation leads to the following expression for the expected fault dimension, where L_0 is the initial value of the fault at time $t = t_0$.

$$E\left[L(t)\right] = L_0 \exp\left(\gamma_0 (t - t_0)\right) \tag{28}$$

Now, consider a value for the fault dimension $L_{\mathrm{lim}} = L(t_{\mathrm{RUL}})$ where t_{RUL} is the predicted mean RUL. An illustration showing the time-evolution of the expected fault growth model from (27) is presented in Figure 13 where t_0, t_{RUL}, L_0 and L_{lim} are labeled accordingly. The RUL is computed by projecting the intersection of L_{lim} and the expectation of the fault dimension trajectory, $E\left[L\left(t\right)\right]$, onto the time axis as shown. Control boundaries for a given t_{RUL} corresponding to a particular motor current, u_{RUL}, are found and used as soft cost constraints in the MPC cost function J, discussed in the next section.

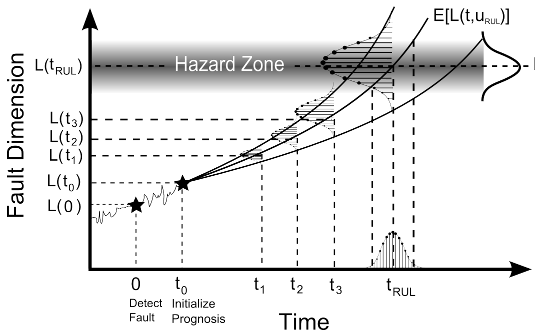

Figure 13: Prognosis prediction of fault dimension highlighting the control input corresponding to the targeted RUL.

4.2 Model Predictive Controller

The MPC formulation presented in this section maximizes the system performance by minimizing the tracking error between the desired set point $\mathbf{r}$ and the measured plant output $\mathbf{y}$. (Cairano *et al.*, 2007; Camacho and Bordons, 2004; Qin and Badgwell, 2003; Maciejowski, 2002)

System Model

A general non-linear state equation can be expressed as (29) where $\mathbf{x}$, $\mathbf{u}$, $\mathbf{d}$, $\mathbf{v}$ and $\mathbf{w}$ represent the model states, control input, measured disturbance, measured noise and process noise, respectively. An illustration of the non-linear system with MPC is provided in Figure 14.

$$\begin{cases} \mathbf{x}\left(t+1\right) &= f_m\left(\mathbf{x},\mathbf{u},\mathbf{v}\right) \\ \mathbf{y}\left(t\right) &= h_m\left(\mathbf{x},\mathbf{u},\mathbf{v},\mathbf{w}\right) \end{cases} \tag{29}$$

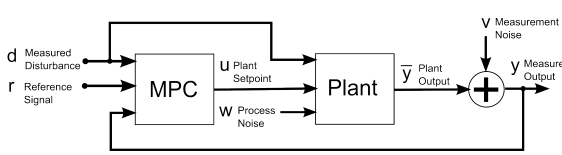

Figure 14: Block diagram of MPC with plant and signals

Cost Function

The MPC is obtained by solving the optimization problem,

$$J=\int_{t_k}^{t_{k+1}}\Big[\left(\mathbf{r}-\mathbf{y}\right)^{\top}\mathbf{Q}\left(\mathbf{r}-\mathbf{y}\right)+\Delta\mathbf{u}^{\top}\mathbf{R}\Delta\mathbf{u}\Big]dt+\rho_{\epsilon}\epsilon^2 \tag{30}$$

where the variables $\mathbf{r}$, $\mathbf{y}$ and $\Delta\mathbf{u}$ correspond to the input reference, plant output and control correction. The soft control boundaries, u_{RUL}, corresponding to a particular t_{RUL} are introduced implicitly in the MPC cost function through the terminal cost. The terminal cost term is comprised of a terminal weight ρ_ϵ and the slack variable ϵ. The weight matrices $\mathbf{Q}$ and $\mathbf{R}$ are defined a-priori as the inverse of the maximum allowable tracking error and control correction, respectively.

Discrete MPC Cost Function

The discretized version of the MPC is defined as,

$$\min_{\Delta(k\,|\,k)\ldots\Delta(m-1+k\,|\,k)}\Big[J\left(\Delta\mathbf{u},\mathbf{r},\mathbf{y}\right)\Big] \tag{31}$$

using the cost function,

$$\begin{aligned} J=\sum_{i=0}^{p-1}\Bigg[&\sum_{j=0}^{n_y}\left|w_{i+1,j}^{y}\,y_j\left(k+i+1|j\right)-r_j\left(k+i+1\right)\right|^2 \\ &+\sum_{j=1}^{n_u}\left|w_{i,j}^{\Delta u}\,\Delta u_j\left(k+i\,|\,k\right)\right|^2\Bigg]+\rho_\epsilon\epsilon^2 \end{aligned} \tag{32}$$

where the subscript "$()_j$" denotes the j-th component of a vector, "$(k+i\,|\,k)$" denotes the value predicted for time $k+i$ based on the information available at time k; $r\left(k\right)$ is the current sample of the output reference subject to,

$$\begin{cases} y\left(k+i+1|k\right) \in \left[y_{j,\min}\left(i\right),y_{j,\max}\left(i\right)\right] \\ u\left(k+i|k\right) \in \left[u_{j,\min}\left(i\right),u_{j,\max}\left(i\right)\right] \\ \Delta u\left(k+i|k\right) \in \left[\Delta u_{j,\min}\left(i\right),\Delta u_{j,\max}\left(i\right)\right] \\ y\left(k+i+1|k\right) \in \left[y_{\min}^{\text{RUL}}-\epsilon V_{\min}^{\text{RUL}},y_{\max}^{\text{RUL}}+\epsilon V_{\max}^{\text{RUL}}\right] \end{cases} \tag{33}$$

s.t. $i\in(0,p-1)$, $h\in[m,p-1]$, $\epsilon>0$ and $m\leq p-1$ with respect to the sequence of input increments $\{\Delta\left(k\,|\,k\right)\ldots\Delta\left(m+k-1\,|\,k\right)\}$ and to the slack variable ϵ and by setting $u\left(k\right)=u\left(k-1\right)+\Delta u\left(k\,|\,k\right)^*$, where $\Delta u\left(k\,|\,k\right)^*$ is the first element of the optimal sequence. In matrix form, the MPC cost function can be written as,

$$J=(\tilde{\mathbf{y}}_p-\tilde{\mathbf{r}}_p)^{\top}\mathbf{W}_y^2(\tilde{\mathbf{y}}_p-\tilde{\mathbf{r}}_p)+\Delta\tilde{\mathbf{u}}_p^{\top}\mathbf{W}_{\Delta u}^2\Delta\tilde{\mathbf{u}}_p+\rho_\epsilon\epsilon^2 \tag{34}$$

Weights

Weights for the optimal control problem in (33) are represented as $\mathbf{W}_u$, $\mathbf{W}_{\Delta u}$ and ρ_ϵ. The weights of each term relate to the emphasis placed on the performance of the system tracking error, level of control correction, and prognosis, respectively.

Hard Constraints

The real-valued constraints y_{min}, y_{max}, u_{min}, u_{max}, Δu_{min}, and Δu_{max} set the absolute lower and upper bounds on the variables y, u and Δu, respectively.

Soft Constraints

The prognosis-based constraints on the internal states $\mathbf{x}_{\text{min}}^{\text{RUL}}$ and $\mathbf{x}_{\text{max}}^{\text{RUL}}$ are introduced as "soft" boundaries through a slack variable ϵ. Violations in the soft boundaries are introduced as the quadratic terminal cost in (33). The constants $V_{\min}^{\text{RUL}}$ and $V_{\max}^{\text{RUL}}$ are non-negative entries which represent the concern for relaxing the corresponding constraint; the larger V^{RUL}, the softer the constraint. For example, setting $V^{\text{RUL}}=0$ implies that the constraint is a hard constraint that cannot be violated.

The MPC Algorithm

Consider for simplicity the prediction model given by:

$$\begin{cases} \mathbf{x}(k+1) &= \mathbf{A}\mathbf{x}(k) + \mathbf{B}\mathbf{u}(k) + \mathbf{w}(k) \\ \mathbf{y}(k) &= \mathbf{C}\mathbf{x}(k) + \mathbf{v}(k) \end{cases} \tag{35}$$

where $\mathbf{A} \in \mathbb{R}^{n_x \times n_x}$, $\mathbf{B} \in \mathbb{R}^{n_x \times n_u}$, $\mathbf{C} \in \mathbb{R}^{n_y \times n_x}$, $\mathbf{x} \in \mathbb{R}^{n_x}$ and the initial conditions for the state variable $\mathbf{x}$ and control input $\mathbf{u}$ are defined as $\mathbf{x}_0 = x(0)$ and $\mathbf{u}_{-1} = u(0^-)$. Then, the prediction of the future trajectories of the model starting at time $k = 0$ is,

$$y(i|0) = \mathbf{C}\left[\mathbf{A}^i\mathbf{x}(0) + \sum_{k=0}^{i-1}\mathbf{A}^{i-1}\mathbf{B}\cdot\ldots \left(\sum_{j=0}^{h}\delta\mathbf{u}(j) + \mathbf{w}(h)\right)\right] + \mathbf{w}(i) \tag{36}$$

which, written in vector form gives,

$$\tilde{\mathbf{y}}_p = \mathbf{S}_x\mathbf{x}_0 + \mathbf{S}_{u1}\mathbf{u}_{-1} + \mathbf{S}_u\Delta\tilde{\mathbf{u}}_p + \mathbf{H}_w\tilde{\mathbf{w}}_p + \mathbf{H}_v\tilde{\mathbf{v}}_p \tag{37}$$

Consider the deterministic case where the random variables and are both omitted from the plant dynamics in (35). The corresponding cost function in (34) can be expressed as,

$$J = \mathbf{k}_r\Delta\tilde{\mathbf{u}}_p + \Delta\tilde{\mathbf{u}}_p^\top\mathbf{K}_{\Delta u}\Delta\tilde{\mathbf{u}}_p + \rho_\epsilon\epsilon^2 + \text{const.} \tag{38}$$

Where the matrices $\mathbf{k}_r$ and $\mathbf{K}_{\Delta u}$ are functions of $\mathbf{A}$, $\mathbf{B}$, $\mathbf{C}$, $\mathbf{x}_0$ and $\mathbf{u}_{-1}$. Now, reconsider the inequality constraints from (33) which can be written in matrix form as,

$$\mathbf{M}_z\tilde{\mathbf{z}}_p \le \mathbf{c}_z \tag{39}$$

where $\tilde{\mathbf{z}}_p = \begin{bmatrix} \Delta\tilde{\mathbf{u}}_p & \epsilon \end{bmatrix}^\top \in \mathbb{R}^{p+1}$ absorbs the slack variable into the constraint optimization problem. Now, define a linear constraint mapping $\mathbf{g}_z : \mathbb{R}^{p+1} \to \mathbb{R}^{6p}$,

$$\mathbf{g}_z(\tilde{\mathbf{z}}_p) = \mathbf{M}_z\Delta\tilde{\mathbf{z}}_p - \mathbf{c}_z \tag{40}$$

Next, define the LaGrangian $L_z : \mathbb{R}^{p+1} \to \mathbb{R}$,

$$L_z(\tilde{\mathbf{z}}_p) = \mathbf{k}_z\tilde{\mathbf{z}}_p + \tilde{\mathbf{z}}_p^\top\mathbf{K}_z\tilde{\mathbf{z}}_p \tag{41}$$

where $\mathbf{k}_z = \begin{bmatrix} \mathbf{k}_r & 0 \end{bmatrix}^\top \in \mathbb{R}^{1\times(p+1)}$ and $\mathbf{K}_z = \text{diag}(\mathbf{K}_{\Delta u}, \rho_\epsilon) \in \mathbb{R}^{(p+1)\times(p+1)}$. The constraints on the system dynamics can be adjoined to the LaGrangian L_z by introducing time-varying LaGrange multiplier vector λ with $\mathbf{g}_z$. The result is the Hamiltonian function,

$$H_\lambda = \mathbf{k}_z\tilde{\mathbf{z}}_p + \tilde{\mathbf{z}}_p^\top\mathbf{K}_z\tilde{\mathbf{z}}_p + \lambda^\top(\mathbf{M}_z\tilde{\mathbf{z}}_p - \mathbf{c}_z) \tag{42}$$

By taking the partial derivative of H with respect to $\tilde{\mathbf{z}}_p$,

$$\frac{\partial H_z}{\partial\tilde{\mathbf{z}}_p} = \mathbf{k}_z + 2\tilde{\mathbf{z}}_p^\top\mathbf{K}_z + \lambda^\top M_z \tag{43}$$

Finally, by setting (43) identically equal to zero, the optimal solution $\mathbf{z}_p^\star$ can be expressed as,

$$\mathbf{z}_p^\star = -\frac{1}{2}\mathbf{K}_z^{-1}\left(\mathbf{k}_z^\top + \mathbf{M}_z\lambda^\star\right) \tag{44}$$

where $\lambda^\star$ satisfies the following Kuhn-Tucker conditions (45) (Fletcher, 2000) for optimality,

$$\begin{cases} \mathbf{M}_z\tilde{\mathbf{z}}_p - \mathbf{c}_z &\le \mathbf{0} \\ \mathbf{k}_z + 2\tilde{\mathbf{z}}_p^\top\mathbf{K}_z + \left(\lambda_p^\star\right)^\top\mathbf{M}_z &= \mathbf{0} \\ \lambda_p^\star\mathbf{g}_z &= 0 \\ \lambda_p^\star &\ge \mathbf{0} \end{cases} \tag{45}$$

Several algorithms exist for solving the linear inequality constraints posed by the MPC such as the Dantiz-Wolfe algorithm (Bemporad *et al.*, 2004).

4.3 Simulation Results

The time-evolution of the turn-to-turn winding faults for different operating conditions were simulated in Simulink using (28).

The model parameters $\bar{a}_m$ and $\bar{b}_m$ were computed using the following equation,

$$\begin{cases} \bar{a}_m &= -\frac{1}{R_{wa}C_{wa}} \\ \bar{b}_m &= \frac{R_0}{R_{wa}} \end{cases} \tag{46}$$

Using these modeling parameters, the fault dimension trajectories were generated for different motor currents, as shown in Figure 15. The initial fault condition was set to $L_0 = 0.05$ for each trajectory.

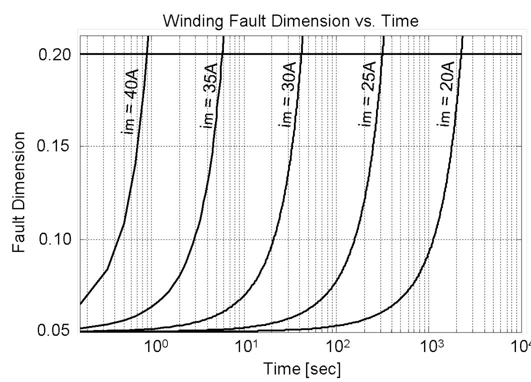

Figure 15: Fault dimension trajectories for different current values.

Notice, as the operating current decreases, the trajectory becomes longer for the same initial fault condition. The horizontal line in Figure 15 denotes the hazard zone. The hazard zone defines the maximum allowable value for the fault dimension. The intersection of the hazard zone with each fault dimension trajectory can be used to determine the expected RUL. The expected RUL computed from Figure 15 for each operating condition is provided in Table 1.

According to Figure 15 the expected RUL is inversely proportional to the magnitude of the operating current. Thus, the RUL can be extended by reducing the operating current. The MPC controller discussed earlier takes advantage of this relationship by reducing

Table 1: Simulation results for the fault-growth model.

Motor Current [A]	RUL [min]	ΔRUL [min]
20	2200	2444
25	310	344.4
30	41.0	45.56
35	6.00	6.667
40	0.90	1.000

the operating current magnitude based on the RUL requirement. The degree of relaxation is dependent on the weight matrices chosen during the controller design phase. To demonstrate the feasibility of the approach the MPC toolbox in MATLAB was used to expedite the design process. The MPC controller contained the variables listed in Table 2. In addition, each constraint has an associated cost as defined in Table 3.

Table 2: Variable types.

Sym	Description	Constraint	Min	Max
θ_{ref}	Reference pos.	Hard	-120°	120°
θ_l	Actuator pos.	Hard	-120°	120°
i_m	Motor current	Soft	-40A	40A

Table 3: Cost function weighting factors used in the simulation.

Symbol	Description	Weight	DoS
$\theta_{\text{ref}} - \theta_l$	Position Error	$[(30/\pi)\,/100]^2$	0
i_m	Motor Current	$[1/40]^2$	0
ϵ	Soft Violation	1	1

The actuator was simulated using the 5th order actuator model from (1). Results for three different fault scenarios were generated using the MPC (parameters given in Table 4) with the corresponding boundaries and weights defined in Tables 2 and 3, respectively. The results are provided in Figure 16. Notice, as the fault dimension increases (left-to-right), the MPC places more emphasis on reducing the magnitude of the motor current. As a consequence, the rise time of the actuator position increases and the magnitude of the winding temperature decreases thereby increasing the estimated RUL.

5 CONCLUSIONS

Fault-tolerant and reconfigurable control strategies for improved critical system reliability and survivability under fault/failure conditions has attracted the attention of the controls community in recent years. To apply these technologies it is essential the system health status be monitored continuously and incipient failures be tracked so that remedial action can be taken as soon as possible to assure its safety. Control reconfiguration at the component level, constitutes the first level of the hierarchical framework for fault-tolerance. The reconfigurable control framework was evaluated using an EMA Simulink model. The results acquired from the simulation demonstrated the feasibility of the approach. Finally, complexity issues must be addressed for specific application domains. Other modules of the integrated fault-tolerant control hierarchy, such as the control redistribution, mission adaptation, etc., are not addressed in this paper but they contribute significantly towards the development of high-confidence systems.

ACKNOWLEDGMENT

This work was supported by the United States National Aeronautics and Space Administration (NASA) under STTR Contract NNX08CD31P. The program is sponsored by the NASA Ames Research Center (ARC), Moffett Field, California 94035. Dr. Kai Goebel, NASA ARC, Dr. Bhaskar Saha, MCT, NASA ARC and Dr. Abhinav Saxena, RIACS, NASA ARC, are the Technical POCs and Liang Tang is the Principal Investigator and Project Manager at Impact Technologies.

NOMENCLATURE

Table 4: List of commonly used symbols.

Sym	**Units**	**Value**	**Description**
$\hat{a}_m$	$\frac{1}{\text{s}}$	–	Thermal parameter
$\hat{b}_m$	$\frac{{}^\circ\text{K}}{\text{s}\cdot A^2}$	-	""
b_ℓ	$\frac{\text{in}\cdot\text{lbf}}{\text{rad/s}}$	2.50×10^{-1}	Load damping
b_m	$\frac{\text{in}\cdot\text{lbf}}{\text{rad/s}}$	1.00×10^{-4}	Motor damping
i_m	A	-	Motor current
k_B	$\frac{\text{eV}}{{}^\circ\text{K}}$	8.62×10^{-5}	Boltzmann's constant
k_{cs}	$\frac{\text{rad}}{\text{rad}}$	1.00×10^{5}	Coupling stiffness
k_e	$\frac{\text{V}}{\text{rad/s}}$	1.10×10^{-1}	Back-emf coefficient
k_ℓ	$\frac{\text{in}\cdot\text{lbf}}{\text{rad}}$	2.00×10^{-3}	Load stiffness
k_{p1}	$\frac{\text{V}}{\text{rad/s}}$	1	Controller gain
k_{p2}	$\frac{1}{\text{s}}$	1	""
k_{p3}	$\frac{\text{rad}}{\text{rad}}$	100	""
k_t	$\frac{\text{in}\cdot\text{lbf}}{\text{A}}$	1.01	Motor torque coefficient
$\tilde{\mathbf{r}}_p$	-	-	Reference array
t_{RUL}	s	-	RUL
y^{RUL}	-	-	RUL output bound
u_{-1}	-	-	Set-point i.c.
$\mathbf{w}_i^u$	-	-	Wt. vector for u
$\mathbf{w}_i^{\Delta u}$	-	-	Wt. vector for Δu
$\mathbf{w}_i^y$	-	-	Wt. vector for y
$\tilde{\mathbf{y}}_p$	-	-	Measurement array

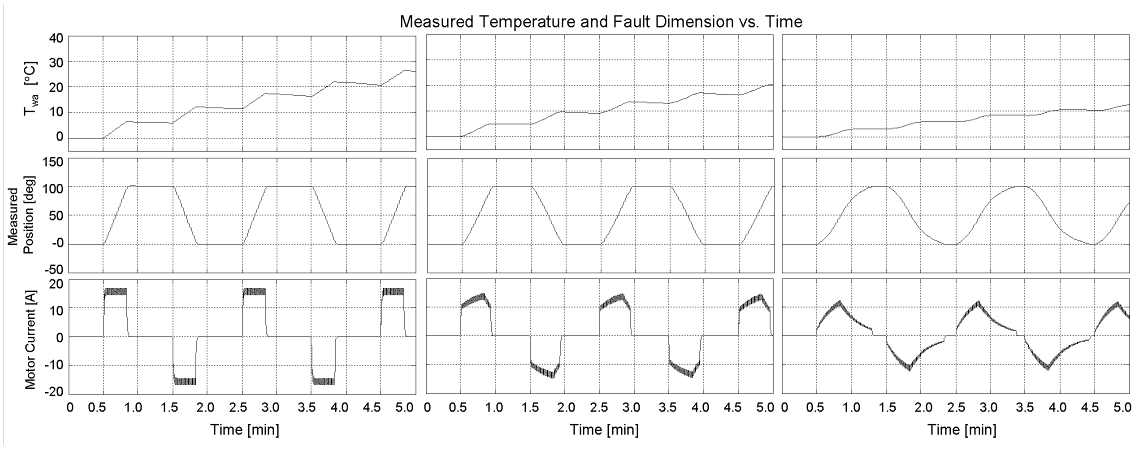

(a) (b) (c)

Figure 16: Simulation results for the reconfigurable control with initial fault dimensions (a) $L_0 = 1 \times 10^{-6}$ (b) $L_0 = 1 \times 10^{-2}$ and (c) $L_0 = 1 \times 10^{-1}$

$\mathbf{z}$	-	-	Concat. state
C_{wa}	$\frac{\mathrm{W}}{°\mathrm{K/s}}$	5.00×10^{-5}	Thermal capacitance
E_a	eV	7.00×10^{-1}	Activation energy
J_ℓ	$\frac{\mathrm{in \cdot lbf}}{1/\mathrm{s}^2}$	2.00×10^{-3}	Load inertia
J_m	$\frac{\mathrm{in \cdot lbf}}{1/\mathrm{s}^2}$	2.10×10^{-3}	Motor inertia
L_{lim}	-	2.00×10^{-1}	Fault dim. limit
L_{tt}	H	3.00×10^{-4}	Turn/turn inductance
N_{cl}	-	1	Load coupling
N_{cm}	-	1	Motor coupling
R_0	Ω	1.60×10^{-1}	Nominal resistance
R_{tt}	Ω	1.60×10^{-1}	Winding resistance
R_{wa}	$\frac{°\mathrm{K}}{\mathrm{W}}$	7.50×10^{-1}	Thermal resistance
T_{wa}	°K	-	Winding-to-ambient temperature
T_{load}	in·lbf	-	Load torque
V^{RUL}	-	-	Degree-of-softness
$\mathbf{W}_y$	-	-	Tracking error weight
$\mathbf{W}_{\Delta u}$	-	-	Set-point adj. weight
β	$\frac{1}{\mathrm{s}}$	1×10^{-6}	Fault-growth coefficient
ϵ	-	-	Slack var.
λ_p	-	-	LaGrange coefficients
θ_ℓ	rad	-	Load position
θ_m	rad	-	Motor position
ω_ℓ	$\frac{\mathrm{rad}}{\mathrm{s}}$	-	Motor speed
ω_m	$\frac{\mathrm{rad}}{\mathrm{s}}$	-	Load speed
$\Delta\tilde{\mathbf{u}}_m$	-	-	Set-point adj. array

REFERENCES

(Arulampalam *et al.*, 2002) M. S. Arulampalam, S. Maskell, N. Gordon, and T. Clapp. A tutorial on particle filters for online nonlinear/non-gaussian bayesian tracking. *IEEE Transactions on Signal Processing*, 50(2):174–188, 2002.

(Bajpai *et al.*, 2001) G. Bajpai, B. C. Chang, and A. Lau. Reconfiguration of flight control systems for actuator failures. *IEEE Aerospace and Electronic Systems Magazine*, 16(9):29–33, 2001.

(Baybutt *et al.*, 2008) M. Baybutt, S. Nanduri, P. W. Kalgren, D. S. Bodden, N. S. Clements, and S. Alipour. Seeded fault testing and in-situ analysis of critical electronic components in ema power circuitry. In *IEEE Aerospace Conference*, pages 1–12, Big Sky, MT, USA, 2008.

(Bemporad *et al.*, 2004) A. Bemporad, M. Morari, and N. L. Ricker. *Model Predictive Control Toolbox for Matlab*. The Mathworks, Inc., Cambridge, MA, 2004.

(Birdwell *et al.*, 1986) J. D. Birdwell, D. A. Castanon, and M. Athans. On reliable control system designs. *IEEE Transactions on Systems, Man and Cybernetics*, SMC-16(5):703–711, September/October 1986.

(Birdwell, 1978) J. D. Birdwell. *On Reliable Control System Designs*. PhD thesis, Department of Electrical Engineering, Massachusetts Institute of Technology, Cambridge, MA, May 1978.

(Bodden *et al.*, 2007) D. S. Bodden, N. S. Clements, B. Schley, and G. Jenney. Seeded failure testing and analysis of an electro-mechanical actuator. In *IEEE Aerospace Conference*, Big Sky, MT, USA, March 3-10, 2007.

(Bogdanov *et al.*, 2006) A. Bogdanov, S. Chiu, L.U. Gokdere, and W. Vian, J. Stochastic optimal control of a servo motor with a lifetime constraint,. In *Proceedings of the 45th IEEE Conference on Decision & Control*, pages 4182–4187, December 2006.

(Boskovic and Mehra, 2001) J. Boskovic and R. Mehra. Hybrid fault-tolerant control of aerospace vehicles. In *Proceedings of the 2001 IEEE International Conference on Control Applications*, pages 441–446, September 2001.

(Brown *et al.*, 2008) D. W. Brown, D. Edwards, G. Georgoulas, B. Zhang, and G. Vachtsevanos. Real-time fault detection and accommodation for cots resolver position sensors. In *1st International Conference on Prognostics and Health Management (PHM)*, Denver, CO, USA, October 6-9, 2008.

(Brown *et al.*, 2009) D. Brown, G. Georgoulas, H. Bae, R. Chen, Y. H. Ho, G. Tannenbaum, J. B. Schroeder, and G. Vachtsevanos. Particle filter based anomaly detection for aircraft actuator systems. In *IEEE Aerospace Conference*, Big Sky, MT, USA, March 7-14, 2009.

(Cairano *et al.*, 2007) S. Di Cairano, A. Bemporad, I. Kolmanovsky, and D. Hrovat. Model predictive control of magnetically actuated mass spring dampers for automotive applications. *International Journal of Control*, 80(11):1701–1716, November 2007.

(Camacho and Bordons, 2004) Eduardo F. Camacho and Carlos Bordons. *Model Predictive Control*. Springer-Verlag, 2nd edition, 2004. ISBN 978-1-85-233694-3.

(Clements *et al.*, 2000) N.S. Clements, B.S. Heck, and G. Vachrsevanos. Component based modeling and fault tolerant control of complex systems. In *Proceedings of the 19th Digital Avionics Systems Conference*, volume 2, pages 6F4/1–6F4/4, October 7-13, 2000.

(Clements, 2003) N. S. Clements. *Fault Tolerant Control of Complex Dynamical Systems*. PhD thesis, School of Electrical and Computer Engineering, Georgia Institute of Technology, Atlanta, GA 30332 USA, April 2003.

(Doucet *et al.*, 2000) A. Doucet, S. Godsill, and C. Andrieu. On sequential monte carlo sampling methods for bayesian filtering. *Statistics and Computing*, 10(3):197–208, 2000.

(Drozeski and Vachtsevanos, 2005) G. Drozeski and G. Vachtsevanos. A fault-tolerant architecture with reconfigurable path planning applied to an unmanned rotorcraft. In *Proceedings of the American Helicopter Society 61st Annual Forum*, June 2005.

(Drozeski *et al.*, 2005) G. Drozeski, B. Saha, and G. Vachtsevanos. A fault detection and reconfigurable control architecture for unmanned aerial vehicles. In *Proceedings of the IEEE Aerospace Conference*, Big Sky, MT, USA, March 2005.

(Filippetti *et al.*, 2000) F. Filippetti, G. Franceschini, C. Tassoni, and P. Vas. Recent developments of induction motor drives fault diagnosis using ai techniques. *IEEE Transactions on Industrial Electronics*, 47(5):994–1004, October 2000.

(Fletcher, 2000) R. Fletcher. *Practical Methods of Optimization*. John Wiley & Sons Ltd., New York, NY, USA, 2nd edition, May 2000. ISBN 978-0-471-49463-8.

(Gokdere *et al.*, 2006) L. U. Gokdere, A. Bogdanov, S. L. Chiu, K. J. Keller, and J. Vian. Adaptive control of actuator lifetime. In *IEEE Aerospace Conference*, March 2006.

(Guler *et al.*, 2003) M. Guler, S. Clements, L. Wills, B. Heck, and G. Vachtsevanos. Generic transition management for reconfigurable hybrid control systems. *IEEE Control Systems Magazine*, 23(1):36–49, February 2003.

(Gutierrez *et al.*, 2003) L. B. Gutierrez, G. Vachtsevanos, and B. Heck. A hierarchical/intelligent control architecture for unmanned aerial vehicles. In *Proceedings of 11th Mediterranean Conference on Control and Automation MED*, Rhodes, Greece, June 2003.

(Heck *et al.*, 2003) B. Heck, L. Wills, and G. Vachtsevanos. Software technology for implementing reusable, distributed control systems. *IEEE Control Systems Magazine*, 23(1):21–35, February 2003. Outstanding Paper Award.

(Hines *et al.*, 2003) W. W. Hines, D. C. Montgomery, D. Goldsman, and C. Borror. *Probability and Statistics in Engineering*. John Wiley and Sons, 4th edition, 2003. ISBN 978-0-471-24087-7.

(Hovakimyan, 2008) N. Hovakimyan. Adaptive control lecture notes. School of Electrical and Computer Engineering, Georgia Institute of Technology, Atlanta, GA 30332 USA, March 2008.

(Isermann, 1984) R. Isermann. Process fault detection based on modeling and estimation methods - a survey. *Automatica*, 20(4):387–404, 1984.

(Isermann, 1997) R. Isermann. Supervision, fault-detection and fault diagnosis methods – an introduction. *Journal of Control Engineering Practice*, 5(5):639–652, May 1997.

(Kamen *et al.*, 1994) E. W. Kamen, G. J. Vachtsevanos, A. Doustmohammadi, and W. Mahmood. A hybrid analytical/intelligent approach to the modeling and control of deds. In *Proceedings of the IEEE/IFAC Joint Symposium on Computer-Aided Control System Design*, March 1994.

(Kleer and Williams, 1987) J. De Kleer and B. C. Williams. Diagnosing multiple faults. *Artificial Intelligence*, 32(1):97–130, 1987.

(Kutner *et al.*, 2004) Michael Kutner, Christopher Nachtsheim, John Neter, and William Li. *Applied Linear Statistical Models*. McGraw Hill, 5th edition, 2004. ISBN 978-0-39059-173-9.

(Levis, 1987) A. H. Levis. Challenges to control: A collective view. *IEEE Transactions on Automatic Control*, AC-32:275–285, 1987.

(Liu, 1996) W. Liu. An on-line expert system-based fault tolerant control system. *Expert Systems With Applications*, 11(1):59–64, 1996.

(Maciejowski, 2002) J.M. Maciejowski. *Predictive Control with Constraints*. Prentice-Hall, Pearson Education Limited, Harlow, UK, 2002. ISBN 978-0-20-139823-6.

(Malik *et al.*, 1998) N. H. Malik, A. A. Al-Arainy, and M. I. Quereshi. *Electrical Insulation in Power Systems*. Marcel Dekker, Inc., New York, NY, 1998.

(Monaco *et al.*, 2004) J. F. Monaco, Ward D.G., and A. J. D. Bateman. A retrofit architecture for model-based adaptive flight control. In *AIAA 1st Intelligent Systems Technical Conference*, Chicago, IL, USA, September 20-22 2004.

(Mufti and Vachtsevanos, 1995) M. Mufti and G. Vachtsevanos. An intelligent approach to fault detection and identification. In *Proceedings of American Control Conference*, June 1995.

(Murray *et al.*, 2002) A. Murray, B. Hare, and A. Hirao. Resolver position sensing system with integrated fault detection for automotive applications. In *Proceedings of IEEE Sensors*, volume 2, pages 864–869, 2002.

(Nandi and Toliyat, 1999) S. Nandi and H. A. Toliyat. Condition monitoring and fault diagnosis of electrical machines - a review. In *Proceedings of the 34th Annual Meeting of the IEEE Industry Applications*, pages 197–204, 1999.

(Nave, 2008) C. Nave. Resistance: Temperature coefficient. Online, September 8 2008.

(Nestler and Sattler, 1993) H. Nestler and Ph. K. Sattler. On-line estimation of temperatures in electrical machines by an observer. *Electric Power Components and Systems*, 21(1):39–50, January 1993.

(Nguyen and Liu, 1998) D. Nguyen and D. B. Liu. Recovery blocks in real-time distributed systems. In *Proceedings of the Annual Reliability and Maintainability Symposium*, pages 149–154, 1998.

(Orchard *et al.*, 2008) M. Orchard, G. Kacprzynski, K. Goebel, B. Saha, and G. Vachtsevanos. Advances in uncertainty representation and management for particle filtering applied to prognostics. In *1st International Conference on Prognostics and Health Management (PHM)*, Denver, CO, USA, October 6-9, 2008.

(Orchard, 2007) M. Orchard. *A Particle Filtering-based Framework for On-line Fault Diagnosis and Failure Prognosis*. PhD thesis, School of Electrical and Computer Engineering, Georgia Institute of Technology, Atlanta, GA 30332 USA, November 2007.

(Paris and Gomez, 1961) P. C. Paris and W. E. Gomez, M. P. anderson. A rational analytic theory of fatigue. *The Trend in Engineering*, 13(7):9, 1961.

(Penman *et al.*, 1994) J. Penman, H. G. Sedding, B. A. Lloyd, and W. T. Fink. Detection and location of interturn short circuits in the stator windings of operating motors. *IEEE Transactions on Energy Conversion*, 9(4):652–658, December 1994.

(Qin and Badgwell, 2003) S. J. Qin and T. A. Badgwell. A survey of industrial model predictive control technology. *Control Engineering Practice*, 11(11):733–764, July 2003.

(Rausch *et al.*, 2007) R. Rausch, K. Goebel, N. Eklund, and B. Brunell. Integrated fault detection and accommodation: A model-based study. *Journal of Engineering for Gas Turbines and Power*, 129(4):962–969, October 2007.

(Saberi *et al.*, 2000) Ali Saberi, Anton A. Stoorvogel, Peddapullaiah Sannuti, and Henrik Niemann. Fundamental problems in fault detection and identification. *International Journal of Robust and Nonlinear Control*, 10(14):1209–1236, November 2000.

(Schoen *et al.*, 1995) R.R. Schoen, T.G. Habetler, F. Kamran, and R.G. Bartfield. Motor bearing damage detection using stator current monitoring. *IEEE Transactions on Industry Applications*, 31(6):1274–1279, November/December 1995.

(Skormin *et al.*, 1994) V. A. Skormin, J. Apone, and J. J. Dunphy. On-line diagnostics of a self-contained flight actuator. *IEEE Transactions on Aerospace and Electronic Systems*, 30(1):186–196, January 1994.

(Stoustrup *et al.*, 1997) Jakob Stoustrup, M. J. Grimble, and Henrik Niemann. Design of integrated systems for the control and detection of actuator/sensor faults. *Sensor Review*, 17(2):38–149, 1997.

(Tang *et al.*, 2008) Liang Tang, Gregory J. Kacprzynski, Kai Goebel, Abhinav Saxena, Bhaskar Saha, and George Vachtsevanos. Prognostics-enhanced automated contingency management for advanced autonomous systems. In *1st International Conference on Prognostics and Health Management (PHM)*, pages 1–9, Denver, CO, USA, October 6-9, 2008.

(Tavner and Penman, 1987) P. J. Tavner and J. Penman. *Condition Monitoring of Electrical Machines*. Research Studies Press, 1987. ISBN 978-0-86341-741-2.

(Vachtsevanos *et al.*, 2005) G. Vachtsevanos, L. Tang, G. Drozeski, and L. Gutierrez. From mission planning to flight control of unmanned aerial vehicles: Strategies and implementation tools. *Annual Reviews in Control*, 29(1):101–115, April 2005.

(Ward *et al.*, 2001) D. G. Ward, J. F. Monaco, R. L. Barron, and R. A. Bird. System for improved receding-horizon adaptive and reconfigurable control, March 2001.

(Watanabe and Himmelblau, 1982) K. Watanabe and D. M. Himmelblau. Instrument fault detection in systems with uncertainties. *International Journal on System Science*, 13:137–158, 1982.

(Willsky, 1976) A. S. Willsky. A survey of design methods for failure detection in dynamic systems. *Automatica*, 12(6):601–611, 1976.

(Wu *et al.*, 2004) B. Wu, S. Abhinav, T. Khawaja, and S. Panagiotis. An approach to fault diagnosis of helicopter planetary gears. In *IEEE Autotestcon*, San Antonio, TX, USA, September 20-23, 2004.

(Wu, 1997) N. E. Wu. Robust feedback design with optimized diagnostic performance. *IEEE Transactions on Automatic Control*, 42(9):1264–1268, September 1997.

(Xianrong *et al.*, 2003) C. Xianrong, V. Cocquempot, and C. Christophe. A model of asynchronous machines for stator fault detection and isolation. *IEEE Transactions on Industrial Electronics*, 50(3):578–584, June 2003.

(Yavrucuk *et al.*, 1999) I. Yavrucuk, J. V. R. Prasad, and S. V. Hanagud. Reconfigurable flight control using rpm control for heli-uav's. In *Proceedings of the 25th European Rotocraft Forum*, 1999.

(Ye and Yang, 2006) Dan Ye and Guang-Hong Yang. Adaptive fault-tolerant tracking control against actuator faults with application to flight control. *IEEE Transactions on Control Systems Technology*, 14(6):1088–1096, November 2006.

(Zhang and Jiang, 2003) Y. Zhang and J. Jiang. Bibliographical review on reconfigurable fault-tolerant control systems. In *Proceeding of the SAFEPROCESS 2003: 5th Symposium on Detection and Safety for Technical Processes*, pages 265–276, Washington D.C., USA, 2003.

(Zhang *et al.*, 2008a) B. Zhang, G. Georgoulas, M. Orchard, A. Saxena, D. Brown, G. Vachrsevanos, and S. Liang. Rolling element bearing feature extraction and anomaly detectioni based on vibration monitoring. In *16th Mediterranean Conference on Control and Automation*, Ajaccio, France, June 25-27, 2008.

(Zhang *et al.*, 2008b) B. Zhang, C. Sconyers, C. Byington, R. Patrick, M. Orchard, and G. Vachtsevanos. Anomaly detection: A robust approach to detection of unanticipated faults. In *1st International Conference on Prognostics and Health Management (PHM)*, Denver, CO, USA, October 6-9, 2008.

(Zhou *et al.*, 1996) K. Zhou, J. C. Doyle, and K. Glover. Robust and optimal control. In *Proceedings of the 35th IEEE Decision and Control*, Kobe, Japan, December 11-13, 1996.

Douglas W. Brown received the B.S. degree in electrical engineering from the Rochester Institute of Technology in 2006 and the M.S degree in electrical engineering from the Georgia Institute of Technology in 2008. He is a recipient of the National Defense Science and Engineering Graduate (NDSEG) Fellowship and is currently pursuing the Ph.D. degree in electrical engineering at the Georgia Institute of Technology specializing in control systems. His research interests include incorporation of Prognostics Health Management (PHM) for fault-tolerant control. Prior to joining Georgia Tech, Douglas was employed as a project engineer at Impact Technologies where he worked on incipient fault detection techniques, electronic component test strategies, and diagnostics/prognostic algorithms for power supplies and RF component applications.

George Georgoulas received Diploma and PhD degrees from the Department of Electrical and Computer Engineering, University of Patras, Patras in 1999 and 2006, respectively. He joined the ICSL in October 2006 as a postdoctorate. His research interests include intelligent data analysis and development of decision support systems for complex systems.

Brian M. Bole graduated from the FSU-FAMU School of Engineering in 2008 with a B.S. in ECE and Applied Math. In August 2008 he joined the ISCL, where he is pursuing a PhD in ECE. His research interests include optimal control and fault tolerant control, based on fault diagnosis and prognosis estimates. graduated from the FSU-FAMU School of Engineering in 2008 with a B.S. in ECE and a B.S. in Math. Prior to joining the group he worked at the Florida Department of Transportation Structures Research Center. Brian is interested in robust control schemes utilizing fault prognosis and diagnosis.

Hai-Long Pei is a Professor and Deputy Dean of the College of Automation Science and Engineering at South China University of Technology. He received the B.S. degree and the M. Sc. degree both in electronic engineering from the Northwestern Polytechnical University in China in 1986 and 1989 separately, and the Ph.D. degree in Automation from South China University of Technology in 1992. His research interest includes autonomous systems, intelligent control, and prognosis enhanced reconfiguration control.

Marcos E. Orchard received the B.Sc. degree (1999) from the Catholic University of Chile, Santiago, Chile, and the M.S. (2005) and Ph.D. (2007) degrees in electrical and computer engineering from the Georgia Institute of Technology, Atlanta. He is currently an Assistant Professor with the Department of Electrical Engineering, Universidad de Chile, Santiago, Chile. His current research interests include system identification, statistical process control and the development of real-time frameworks for both fault diagnosis and failure prognosis.

Liang Tang is a Sr. Lead Engineer at Impact Technologies LLC, Rochester, NY. His research interests include diagnostics, prognostics and health management systems (PHM), fault tolerant control, intelligent control, and signal processing. He obtained a Ph.D. degree in Control Theory and Engineering from Shanghai Jiao Tong University, China in 1999. Before he joined Impact Technologies, he worked as a post doctoral research fellow at Intelligent Control Systems Laboratory, Georgia Institute of Technology. At Impact Technologies he is responsible for multiple DoD and NASA funded research and development projects on structural integrity prognosis, prognostics and uncertainty management, automated fault accommodation for aircraft systems, and UAV controls. Dr. Tang has published more than 30 papers in his areas of expertise.

Bhaskar Saha is a Research Programmer with Mission Critical Technologies at the Prognostics Center of Excellence, NASA Ames Research Center. His research is focused on applying various classification, regression and state estimation techniques for predicting remaining useful life of systems and their components. He has also published a fair number of papers on these topics. Bhaskar completed his PhD from the School of Electrical and Computer Engineering at Georgia Institute of Technology in 2008. He received his MS from the same school and his B. Tech. (Bachelor of Technology) degree from the Department of Electrical Engineering, Indian Institute of Technology, Kharagpur.

Abhinav Saxena is a Staff Scientist with Research Institute for Advanced Computer Science at the Prognostics Center of Excellence NASA Ames Research Center, Moffet Field CA. His research focus lies in developing and evaluating prognostic algorithms for engineering systems using soft computing techniques. He is a PhD in Electrical and Computer Engineering from Georgia Institute of Technology, Atlanta. He earned his B.Tech in 2001 from Indian Institute of Technology (IIT) Delhi, and Masters Degree in 2003 from Georgia Tech. Abhinav has been a GM manufacturing scholar and is also a member of IEEE, AAAI and ASME.

Kai Goebel received the degree of Diplom-Ingenieur from the Technische Universität München, Germany in 1990. He received the M.S. and Ph.D. from the University of California at Berkeley in 1993 and 1996, respectively. Dr. Goebel is a senior scientist at NASA Ames Research Center where he leads the Diagnostics & Prognostics groups in the Intelligent Systems division. In addition, he directs the Prognostics Center of Excellence and he is the Associate Principal Investigator for Prognostics of NASA's Integrated Vehicle Health Management Program. He worked at General Electric's Corporate Research Center in Niskayuna, NY from 1997 to 2006 as a senior research scientist. He has carried out applied research in the areas of artificial intelligence, soft computing, and information fusion. His research interest lies in advancing these techniques for real time monitoring, diagnostics, and prognostics. He holds ten patents and has published more than 100 papers in the area of systems health management.

George J. Vachtsevanos is a Professor Emeritus of Electrical and Computer Engineering at the Georgia Institute of Technology. He was awarded a B.E.E. degree from the City College of New York in 1962, a M.E.E. degree from New York University in 1963 and the Ph.D. degree in Electrical Engineering from the City University of New York in 1970. He directs the Intelligent Control Systems laboratory at Georgia Tech where faculty and students are conducting research in intelligent control, neurotechnology and cardiotechnology, fault diagnosis and prognosis of large-scale dynamical systems and control technologies for Unmanned Aerial Vehicles. His work is funded by government agencies and industry. He has published over 240 technical papers and is a senior member of IEEE. Dr. Vachtsevanos was awarded the IEEE Control Systems Magazine Outstanding Paper Award for the years 2002-2003 (with L. Wills and B. Heck). He was also awarded the 2002-2003 Georgia Tech School of Electrical and Computer Engineering Distinguished Professor Award and the 2003-2004 Georgia Institute of Technology Outstanding Interdisciplinary Activities Award.